Rapid identification of structural phases in combinatorial thin-film libraries using x-ray diffraction and non-negative matrix factorization

C. J. Long,[1] D. Bunker,[2] X. Li,[2] V. L. Karen,[2] and I. Takeuchi[1]
[1]*Department of Materials Science and Engineering, University of Maryland, College Park, Maryland 20742, USA*
[2]*National Institute of Standards and Technology, Gaithersburg, Maryland 20899, USA*

(Received 1 April 2009; accepted 12 August 2009; published online 2 October 2009)

In this work we apply a technique called non-negative matrix factorization (NMF) to the problem of analyzing hundreds of x-ray microdiffraction (μXRD) patterns from a combinatorial materials library. An in-house scanning x-ray microdiffractometer is used to obtain μXRD patterns from 273 different compositions on a single composition spread library. NMF is then used to identify the unique μXRD patterns present in the system and quantify the contribution of each of these basis patterns to each experimental diffraction pattern. As a baseline, the results of NMF are compared to the results obtained using principle component analysis. The basis patterns found using NMF are then compared to reference patterns from a database of known structural patterns in order to identify known structures. As an example system, we explore a region of the Fe–Ga–Pd ternary system. The use of NMF in this case reduces the arduous task of analyzing hundreds of μXRD patterns to the much smaller task of identifying only nine μXRD patterns. © *2009 American Institute of Physics.* [doi:10.1063/1.3216809]

I. INTRODUCTION

The combinatorial approach has been used to discover new materials phases as well as perform rapid mapping of composition-structure-property relationships in complex materials systems.[1–3] Using thin-film composition spread libraries, large fractions of compositional phase diagrams can be mapped out with a high density of data points on a single wafer.[4–7] Mapping phase diagrams is central to obtaining comprehensive pictures of materials systems, and mapping active physical properties as a function of composition is an integral part of understanding the underlying physical mechanism of the properties.[7–9] Thin-film materials can often display properties with deviation from bulk samples, but it has been shown in many systems that one can indeed obtain compositional trends that closely resemble or mirror those of bulk counterparts.[7,10]

The increasing popularity of the combinatorial approach to material science has resulted in a need to develop new techniques that can be used to analyze large amounts of data in parallel. One type of data that presents a particularly large challenge is x-ray microdiffraction (μXRD) data. It is possible to analyze each spectrum individually, but this process is very tedious and time consuming. In order to reduce the difficulty of this task, we are in the process of developing tools and techniques that can be used to analyze many diffraction spectra at once, instead of the traditional one at a time approach.

In previous work, we have presented our techniques for the visualization of diffraction data from ternary composition libraries[11] as well as our work using clustering analysis to sort spectra into discrete groups.[12] In this work, we apply a technique called non-negative matrix factorization (NMF) to the problem of identifying the unique diffraction patterns present in a set of μXRD spectra, as well as quantifying the contribution of those patterns to each experimental spectrum. As an example system, we look at a region of the Fe–Ga–Pd ternary system.

II. EXPERIMENTAL

Our interest in the Fe–Ga–Pd ternary system stems from the fact that the Fe–Ga and Fe–Pd binary phase diagrams contain compositions with unusual magnetic actuator properties. Fe–Ga is a well-known material system exhibiting large magnetostriction for Ga content between 20 and 30 at. %. The origin of this property is attributed to the complexity of the Fe–Ga binary phase diagram in this region.[13] $Fe_{70}Pd_{30}$ is a ferromagnetic shape memory alloy[14] whose martensitic transition is associated with a magnetic field-induced strain of about 10 000 ppm.[15] Fortunately, Ga and Pd both form solid solutions when they are substituted into the Fe lattice. This means that they could possibly be substituted into the Fe lattice without disturbing the original crystal structure.

Natural thin-film composition spreads of the Fe–Ga–Pd system were deposited at room temperature using an ultrahigh-vacuum three gun magnetron cosputtering system with a base pressure of 10^{-9} Torr (10^{-7} Pa) on 3 in. (76.2 mm) diameter (100) oriented Si wafer. The samples were then postannealed at 650 °C for 2 h in our sputtering chamber. The base pressure during annealing was 10^{-8} Torr. After the deposition, the composition of each sample on the wafer was immediately determined via wavelength dispersive spectroscopy in atomic percent. This measurement can determine the percent fraction of each atom contained at each point on the wafer to better than 1%. Figure 1 shows the schematic

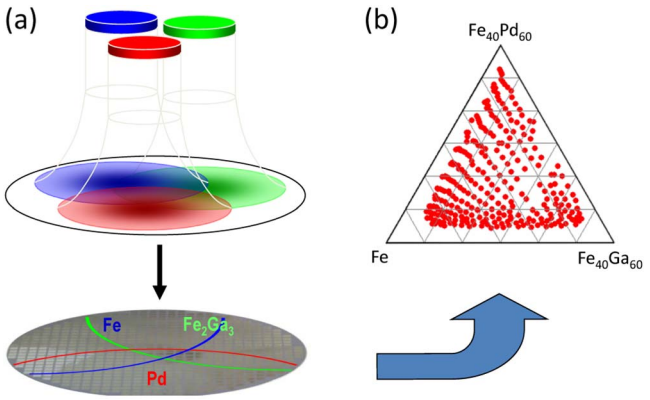

FIG. 1. (Color online) Schematic for the deposition of a thin-film composition library in the Fe–Ga–Pd ternary metallic system. (a) Three sputtering guns in a nonconfocal geometry deposit a continuous gradient of compositions onto a gridded, 3 in. Si wafer. (b) The resulting compositions on the ternary diagram as measured by wavelength dispersive spectroscopy.

procedure for the synthesis of a ternary composition spread that covers the relevant part of the phase diagram.

μXRD of the fabricated films was performed using the ω-scan mode of a D8 DISCOVER[16] for combinatorial screening by Bruker-AXS. The diffractometer was equipped with a HI-STAR two-dimensional detector, which captures data for a fixed range of 2θ and ω at once. The composition spread wafer contained a grid of 535 individual 1.75 mm^2 squares with continuously changing composition. However, μXRD was performed for only 273 of the 535 squares due to time constraints. We used an x-ray beam spot size of 1 mm diameter. Once the data acquisition was complete, the raw detector images were integrated to obtain 2θ angles and peak intensities using the D8 GADDS program and a script to automate the process.

Since there is some extraneous information in the μXRD spectra (e.g., substrate peaks and background signal) some preprocessing was done on the data before it was analyzed. In particular, background subtraction, cropping, and normalization were performed. Background subtraction was done by fitting and subtracting a piecewise polynomial from the data on a spectrum by spectrum basis. After background subtraction, the full measured 2θ range was cropped down to the minimum range such that all of the detected μXRD peaks from all the samples (but not from the substrate) were contained in the spectra. For these Fe–Ga–Pd samples, we found that this range was from 37° to 50°. The spectra were then normalized such that the largest intensity in any given spectrum was unity.

III. NMF OF μXRD DATA

NMF is a relatively new technique, which has been applied to problems in several fields. NMF has been used to perform image segmentation,[17] document clustering,[18] and spectral unmixing of satellite reflectance data,[19] among other applications. To the best of the authors' knowledge, this is the first time that it has been applied to μXRD data.

The basic idea of NMF is to deconvolve a large number of non-negative spectral patterns into a smaller number of non-negative basis patterns. The experimental patterns can then be described as a weighted superposition of the deconvolved basis patterns.

We have two main reasons why we have chosen to use NMF over other multivariate techniques. First, since NMF describes experimental spectra as a superposition of basis patterns, it can easily handle diffraction patterns that result from mixtures of different crystal structures. This makes NMF a good choice when compared to techniques that sort patterns into discreet groups. NMF therefore represents a significant improvement over our previous work using hierarchical clustering analysis.[12] Second, NMF produces basis patterns that can be directly interpreted as diffraction patterns. This makes NMF a more suitable technique when dealing with μXRD data in comparison to principal component analysis (PCA) since PCA produces basis patterns that contain negative values.

In order to perform the factorization, the μXRD data were arranged into an m-by-n matrix, Y, where m is the number of compositions for which μXRD patterns were measured ($m=273$ in this case) and n is the number of angles at which the diffraction intensity was recorded. In this case, the diffraction intensity was measured every 0.02° over the 2θ range from 37° to 50°, so $n=651$. NMF was then used to find an approximate factorization of Y into the product of two smaller matrices, A and X. The matrices A and X are constrained such that they may only contain non-negative values. Any noise in the experimental data or errors in the factorization get accounted for by an error matrix, E, which may contain negative values.

$$Y = AX + E, \quad \text{where } A_{ij} \geq 0 \text{ and } X_{ij} \geq 0.$$

The size of matrix A is m-by-r, the size of matrix X is r-by-n, and the size of matrix E is m-by-n, where r is the rank of the factorization. The rank of the factorization corresponds to the number of basis patterns that are to be extracted from the experimental data, and is chosen by the user of the algorithm. Choosing the correct value for r requires some consideration and is discussed below in the comparison of NMF to PCA. For the μXRD data set presented here, we found that a rank nine factorization produced a good deconvolution of the experimental diffraction patterns.

Each row of the matrix X contains a basis pattern. Each basis pattern contains a set of peaks that tend to appear together in the experimental data. After the factorization is completed, the basis patterns are normalized such that the largest value in each spectrum is unity. The content of the matrix X is presented in Fig. 2.

Each row of the matrix A contains the weights, or linear mixing coefficients, of the basis patterns for a particular experimental pattern. Since the basis patterns are normalized to unit intensity, each matrix element in A corresponds to the intensity of a given basis pattern for a particular experimental pattern. In Figs. 3 and 5, the relative weights of the basis patterns for a given composition are represented using pie charts. The size of each piece of a pie chart corresponds to the amount of each basis pattern present in a given sample.

Each row of the matrix AX contains a deflated version of an experimental spectrum. The spectra are said to be deflated

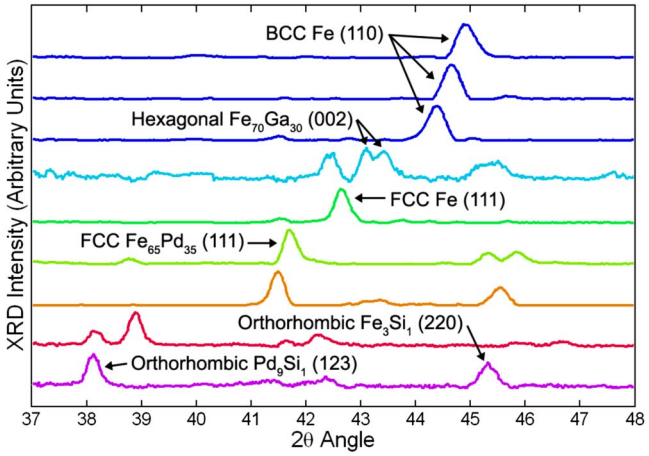

FIG. 2. (Color online) The nine basis patterns found using NMF. The patterns are color coded by structural phase. Peaks identified as possible matches to reference patterns are labeled. The spectra are offset vertically for visibility.

because there is typically a much smaller number of degrees of freedom in the matrix AX than there is in the matrix Y. The number of degrees of freedom in the matrix AX is the number of matrix elements in A plus the number of matrix elements in X. In contrast, the number of degrees of freedom in Y is the number of matrix elements in Y. For example, in the data set explored here, there are 177 723 matrix elements in Y, but only 8316 matrix elements for a rank nine factorization AX. Thus, the dimensionality of the parameter space for the deflated matrix (AX) is less than 5% of that for the experimental data. Ideally, the only difference between the experimental spectra and the deflated spectra should be that the deflated spectra contain much less noise.

Each row of the matrix E contains a residual spectrum,

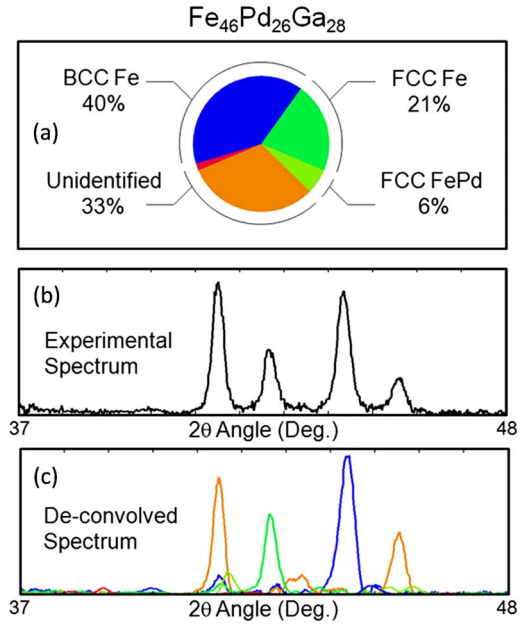

FIG. 3. (Color online) Part (a) shows the weights of the basis patterns which are present the sample with nominal composition of $Fe_{46}Pd_{26}Ga_{28}$. Part (b) shows the experimental μXRD pattern for this sample. Part (c) shows the weighted basis patterns, which provide a deconvolution of the experimental pattern.

which is the difference between an experimental pattern and the corresponding deflated pattern. Ideally, after the factorization, the residual spectra should only contain noise.

Finding the best solution for A and X is equivalent to minimizing the norm of the error matrix. The problem to be solved by the NMF algorithm can thus be stated as

find A and X such that

$$\|E\| = \|Y - AX\| \text{ is a minimum.}$$

There are several possible ways of calculating the norm of E and also several possible NMF algorithms for finding A and X such that $\|E\|$ is minimized. In this work, we calculated the norm of E using the squared Frobenius norm, which is simply the sum of the squared matrix elements. An exhaustive discussion of NMF algorithms is beyond the scope of this work and can be found elsewhere.[20] For our work, suffice to say that we used the regularized alternating least-squares algorithm[21] for finding A and X. The software used to perform the factorization was NMFLAB,[22] which is a third party toolbox for MATLAB.

IV. COMPARISON OF NMF TO PCA

In order to validate the results of the NMF, we must be assured that the NMF algorithm has converged to a global minimum of $\|E\|$, and not merely a local minimum or stationary point. Unfortunately, one of the current limitations of NMF is that convergence to a global minimum is not guaranteed. In order to show that the factorization has converged to very near the global minimum, and in order to choose the correct rank of the factorization, we compare the results of NMF to those of PCA.

The relevant feature of PCA for this work is that for a given rank, PCA finds a matrix factorization that produces the global minimum of the squared Frobenius norm of the error matrix. That is to say, when representing experimental spectra as a linear superposition of basis patterns, PCA produces the best possible approximation to the data using a given number of basis patterns. Since PCA produces a factorization with the minimum possible amount of error, we can assess the quality of the factorization produced using NMF by comparing the amount of information captured by NMF to the amount of information captured using PCA.

It is worth noting that even though PCA produces a matrix factorization that minimizes the Frobenius norm of the error matrix, it does not produce basis patterns that are physically realizable diffraction patterns. Specifically, the basis patterns produced using PCA contain negative values and are all orthogonal to each other. This is not consistent with the solution we are looking for since the diffraction patterns of a set of crystal structures will only contain positive values and are very unlikely to be orthogonal. For this reason, the basis patterns produced by PCA do not form a useful deconvolution for our work. In contrast, the basis patterns produced using NMF contain only non-negative values and are not constrained to be orthogonal. Thus, they are ideally suited for the task of deconvolving diffraction patterns.

A comparison of the amount of experimental data accounted for as a function of the number of basis patterns

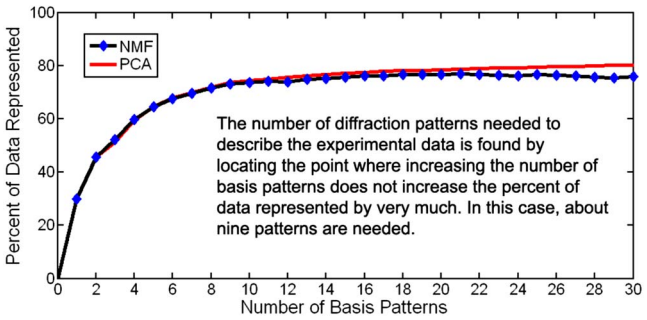

FIG. 4. (Color online) The graph above shows the percent of experimental data that can be represented using a given number of basis patterns. The fraction of the data accounted for using NMF is very near that accounted for using PCA, implying that the factorization produced by NMF is valid. The reason why 100% of the data is not accounted for by the factorizations is that there is noise in the experimental data. In this case, noise accounts for about 20% of the experimental data.

using both PCA and NMF is presented in Fig. 4. The amount of error in the factorization is found by calculating the ratio of the absolute area of all of the residual spectra to the area of all of the experimental spectra,

$$\text{percent of data represented} = 100^{*}\left[1-\sum_{i}^{n}\sum_{j}^{m}|Y_{ij}-(AX)_{ij}|/\sum_{i}^{n}\sum_{j}^{m}Y_{ij}\right].$$

The first point to observe in Fig. 4 is that below about 20 basis patterns, the percent of data explained using NMF is very close to the amount of data explained using PCA. Thus, in this low-rank region we can be satisfied that the employed NMF algorithm has converged to a point that is very near the global minimum of the norm of the error matrix. Above 20 basis patterns, the amount of data explained by NMF begins to diverge from the amount explained by PCA, and can even decrease compared to lower rank factorizations. We believe that this decrease is due to the NMF algorithm falling into a local minimum of the norm of the error matrix instead of converging to the global minimum.

There are techniques available which can reduce the tendency to fall into local minima, although none guarantees that the minima are avoided altogether. The most common approach is to choose many different random initializations for A and X, run NMF using each one, and then keep the best result.[20] Another possibility is to pass the results of one NMF algorithm to another algorithm in the hope that they do not both get stuck in the same minimum.[23] Yet a third approach is to choose the initialization of A and X such that they are already near the global minimum.[24,25] For our case, we are most interested in the low rank factorizations where the local minima did not pose a problem. As a result, we have not focused here on trying to avoid these local minima.

In order to produce an accurate factorization of the experimental data, the correct rank of the factorization must be determined. Determining the correct rank of the factorization corresponds to determining the number of unique patterns that exist in the data. Choosing a rank that is too small will result in basis patterns that are composed of mixtures of pure phase patterns. Choosing a rank that is too large may result in the pattern from a single structural phase being broken up into several basis patterns, each of which contains a subset of the reflections from that structure. Ideally, by choosing the rank of the factorization to match the number of crystal structures, each basis pattern should represent the diffraction pattern of a single crystal structure. We note that there are some cases where each basis pattern will not represent the diffraction pattern of a single crystal structure. These cases are discussed later in the "limitations and future work" section.

Using Fig. 4 we can estimate how many patterns are needed to describe the data. We do this by determining the point where increasing the number of basis patterns does not increase the amount of data explained by very much. In the case of the Fe–Ga–Pd data set, this occurs at about nine basis patterns for both PCA and NMF.

V. RESULTS FOR Fe–Ga–Pd COMPOSITION SPREAD

In Fig. 2, one can see the nine basis patterns found using NMF for this system. There are a couple of features of these patterns that are worth discussing. The first is that there are several patterns that are only present as mixtures in the experimental data, but show up as separate patterns in the extracted basis patterns. This shows that NMF can identify the correct basis patterns even when there are no endmembers present in the data set. The second feature to note is that in the case of bcc Fe, the NMF algorithm extracts several different patterns that correspond to the same structure but where the position of the peak has shifted. This is one limitation of the NMF algorithm. Since the algorithm has no way of accounting for peak shifts, it identifies each shifted pattern as a new pattern. In this case, it is up to the materials scientist to identify that the shifted patterns do not correspond to several different structures, but in fact correspond to a single structure that exhibits a change in lattice parameters as a function of chemical composition.

In order to identify the structural phases corresponding to the basis patterns found using NMF, the basis patterns were compared to a set of reference spectra calculated from the crystallographic databases available at NIST. In particular, we used the Inorganic Crystal Structure Database (ICSD)[26] and the NIST Structural Database.[27] If the composition of the reference pattern was within (or very near) the composition space where a given basis pattern was prevalent, and the peaks were separated by less than 0.4°, then we considered this to be a match. We note that several of the peaks present in the basis patterns produced by NMF contain unidentified peaks. The main reason that not all of the diffraction peaks were identified using this method is that there are a limited number of reference patterns available for comparison in the crystallographic databases. The number of available reference patterns is especially sparse as one moves away from the binary edges of the ternary diagram.

Figure 5 presents a ternary diagram in which the weights of the NMF basis patterns for each composition have been represented as pie charts. Since the basis patterns found using NMF correspond to structural phases, this diagram gives

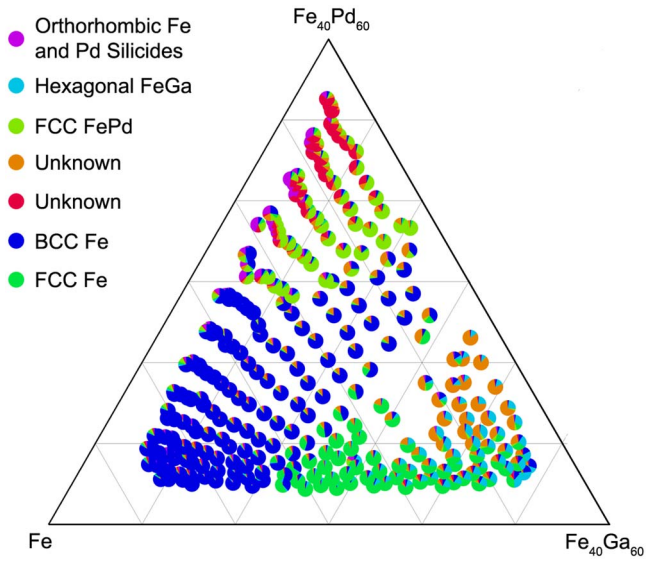

FIG. 5. (Color online) The structural phase diagram produced using the weights of the basis diffraction patterns found using NMF. Each pie chart corresponds to a composition for which μXRD was measured and each piece of the pie chart corresponds to the weight of one of the basis patterns found using NMF. The phase diagram produced in this manner contains a quantitative representation of the phases present throughout the part of the ternary system that we have explored. Possible matches to a database of known patterns are presented at the top left.

us a quantitative distribution of structural phases as a function of composition, including the existence of multiphase regions.

Although the full ternary phase diagram of this system is not available for comparison, the projection of the identified distributions to the two binary (Fe–Ga and Fe–Pd) systems matches the known phase diagrams reasonably well. According to the published equilibrium phase diagrams, in the Fe–Ga system,[28] starting from the pure Fe end, the α-Fe phase persists up to about 80% Fe, beyond which various mixture regions containing the Fe–Ga $L1_2$ phase stretches up to about 50% Fe. The $L1_2$ phase has a fcc structure, which in our study was correctly identified as being isostructural to fcc Fe. In the Fe–Pd system,[29] a mixture of α-Fe and $Fe_{50}Pd_{50}$ is known to extend from 100% Fe to about 50% Fe. It is expected that this region would "appear" as mainly α-Fe. In our study, we find that at approximately $Fe_{65}Pd_{35}$, the dominant phase switches from α-Fe to fcc $Fe_{65}Pd_{35}$, which stretches beyond 50% Fe. Our analysis has identified this region (starting at the correct composition) as the fcc $Fe_{65}Pd_{35}$, which we believe is a quenched phase.

VI. EXISTING PROBLEMS AND FUTURE WORK

The ultimate goal of our efforts is to reach a point where the analysis of hundreds of μXRD spectra automatically identifies all of the pure phases present in a system and quantifies the percent of each phase present for each composition. The work presented here represents significant progress toward this goal, but there are still significant problems left to overcome. Some of these problems are inherent in the use of thin films, while others are particular to the analysis of μXRD data using NMF.

One of the problems one faces when attempting to do structure identification of thin films is that it may simply not be possible to precisely identify all the lattice parameters, and thus, the exact structure of the material. In principle, in order to completely determine the lattice parameters, one must measure the intensity of all x-ray reflections, as in powder diffraction. The films under study here are often at least textured, and are sometimes even epitaxially grown. This texturing reduces the number of reflections to only the ones from the preferred orientations. It is also possible that the film may exhibit different preferred orientations at different sites, resulting in different sets of reflections for the same structure. As a partial solution to the problem of textured films, it is sometimes possible to obtain some additional information about textured samples by tilting the wafer. Other problems include formation of "spurious" phases such as silicides, as observed here. There could also be formation of metastable phases that are unique to the film structures and cannot be synthesized in bulk form.

In addition to the difficulties of working with thin films, there are also problems that are particular to the analysis of μXRD data using NMF. One of the difficulties of quantifying the amount of each phase present in a sample is that the structure factor can be different for each pattern. This results in a difference in the brightness of different patterns. Thus the relative intensities of the patterns present in a sample provided by the NMF weights matrix (and presented in Fig. 5) cannot be directly compared to the volume fraction of the structures present in a sample. It is possible to get around this problem by renormalizing the weights of each basis pattern by the intensity of each pure phase. However this is only possible if for each pure phase there is at least one sample that is not a mixture. A second difficulty that is not addressed by NMF is peak shifting due to changing lattice constants. If there are a number of diffraction patterns across which there is a large shift in the position of a peak, then it will be more profitable for the algorithm to "spend" its basis patterns describing this peak shift, instead of identifying other structural phases. The best that can be achieved in the case of peak shifts using NMF is the identification of several patterns, each corresponding to a different shift. Yet a third weakness is that diffraction patterns that correspond to different preferred orientations of the same structure might be identified as different structures. Often, these problems can be partially solved by manually scrutinizing the basis patterns produced by NMF and/or by applying prior knowledge about the materials.

Future work will be focused on developing a technique that can handle mixtures of phases and can also track peak shifts as a function of composition. We will also focus on the exploration of other ternary systems.

ACKNOWLEDGMENTS

This project is funded in part by NIST's Systems Integration for Manufacturing Applications (SIMA) program. SIMA supports NIST projects applying information technologies and standards-based approaches to manufacturing software integration problems. D. Bunker was supported by

the National Science Foundation's Research Experience for Undergraduates program (Division of Materials Research). This work was supported by NSF MRSEC DMR Grant No. 0520471 and ONR Grant No. N000140610530.

[1] H. Koinuma and I. Takeuchi, Nature Mater. **3**, 429 (2004).
[2] *Combinatorial Materials Synthesis*, edited by I. Takeuchi and X.-D. Xiang (Dekker, New York, 2003).
[3] I. Takeuchi, R. B. van Dover, and H. Koinuma, MRS Bull. **27**, 301 (2002).
[4] T. Fukumura, M. Ohtani, M. Kawasaki, Y. Okimoto, T. Kageyama, T. Koida, T. Hasegawa, Y. Tokura, and H. Koinuma, Appl. Phys. Lett. **77**, 3426 (2000).
[5] I. Takeuchi, W. Yang, K.-S. Chang, M. Aronova, T. Venkatesan, R. D. Vispute, and L. A. Bendersky, J. Appl. Phys. **94**, 7336 (2003).
[6] R. B. van Dover, L. F. Schneemeyer, and R. M. Fleming, Nature (London) **392**, 162 (1998).
[7] I. Takeuchi, O. O. Famodu, J. C. Read, M. A. Aronova, K.-S. Chang, C. Craciunescu, S. E. Lofland, M. Wuttig, F. C. Wellstood, L. Knauss, and A. Orozco, Nature Mater. **2**, 180 (2003).
[8] S.-W. Cheong and H. Y. Hwang, in *Ferromagnetism vs. Charge/Orbital Ordering in Mixed-Valent Manganites: Colossal Magneto-Resistive Oxides*, edited by Y. Tokura (Gordon and Breach, Amsterdam, 2000), p. 237.
[9] A. Damascelli, Z. Hussain, and Z.-X. Shen, Rev. Mod. Phys. **75**, 473 (2003).
[10] M. J. Turchinskaya, L. A. Bendersky, A. J. Shapiro, K. S. Chang, I. Takeuchi, and A. L. Roytburd, J. Mater. Res. **19**, 2546 (2004).
[11] I. Takeuchi, C. J. Long, O. O. Famodu, M. Murakami, J. Hattrick-Simpers, and G. W. Rubloff, Rev. Sci. Instrum. **76**, 062223 (2005).
[12] C. J. Long, J. Hattrick-Simpers, M. Murakami, R. C. Srivastava, I. Takeuchi, V. L. Karen, and X. Li, Rev. Sci. Instrum. **78**, 072217 (2007).
[13] G. Petculescu, K. B. Hathaway, T. A. Lograsso, M. Wun-Fogle, and A. E. Clark, J. Appl. Phys. **97**, 10M315 (2005).
[14] M. Sugiyama, R. Oshima, and F. E. Fujita, Mater. Trans., JIM **25**, 585 (1984).
[15] J. Koeda, Y. Nakamura, T. Fukuda, T. Kakeshita, T. Takeuchi, and K. Kishio, Trans. Mater. Res. Soc. Jpn. **26**, 215 (2001).
[16] Certain commercial materials and equipment are identified in this paper to specify the experimental procedure. In no instance does such identification imply recommendation or endorsement by the National Institute of Standards and Technology or that the material or equipment identified is necessarily the best available for the purpose.
[17] D. D. Lee and H. S. Seung, Nature (London) **401**, 788 (1999).
[18] F. Shahnaz, M. Berry, V. P. Pauca, and R. Plemmons, Inf. Process. Manage. **42**, 373 (2006).
[19] J. Piper, V. P. Pauca, R. J. Plemmons, and M. Giffin, Proceedings of AMOS Technical Conference, Maui, HI, 2004 (unpublished).
[20] M. W. Berry, M. Browne, A. N. Langville, P. V. Pauca, and R. J. Plemmons, Comput. Stat. Data Anal. **52**, 155 (2007).
[21] A. Cichocki and R. Zdunek, Lect. Notes Comput. Sci. **4493**, 793 (2007).
[22] A. Cichocki and R. Zdunek, http://www.bsp.brain.riken.jp/ICALAB/nmflab.html.
[23] C. Ding, T. Lib, and W. Peng, Comput. Stat. Data Anal. **52**, 3913 (2008).
[24] S. Wild, J. Curry, and A. Dougherty, Pattern Recogn. **37**, 2217 (2004).
[25] C. Boutsidis and E. Gallopoulos, Pattern Recogn. **41**, 1350 (2008).
[26] A. Belsky, M. Hellenbrandt, V. L. Karen, and P. Luksch, Acta Crystallogr., Sect. B: Struct. Sci. **B58**, 364 (2002).
[27] NIST Standard Reference Data Program, Gaithersburg, MD 20899.
[28] *Binary Alloy Phase Diagrams*, 2nd ed., edited by T. B. Massalski (ASM International, Ohio, 1990), p. 1064.
[29] *Binary Alloy Phase Diagrams*, 2nd ed., edited by T. B. Massalski (ASM International, Ohio, 1990), p. 1751.